

Impedance Spectroscopy of Porous Silicon and Silicon-Carbon Anodes Produced by Sintering

D. A. Lozhkina^{a,*}, A. M. Rumyantsev^a, and E. V. Astrova^a

^a Ioffe Institute, St. Petersburg, 194021 Russia

*e-mail: darina.lozhka94@gmail.com, east@mail.ioffe.ru

Received October 29, 2019; revised November 5, 2019; accepted November 5, 2019

Abstract—Dry-sintered macroporous Si electrodes for Li-ion batteries are studied for the first time using spectral impedance measurements. The spectra obtained in the lithiated and delithiated states are simulated with an equivalent electrical circuit, the parameters of which reveal the role of electrochemical processes caused by the surface layer of a solid-phase electrolyte (SEI), electric double layer, and diffusion in the solid phase of the electrode material. It is shown that the effective diffusion coefficient of Li in Si grows with increasing degree of lithiation from $D = 6.5 \times 10^{-12}$ to 2.6×10^{-10} cm²/s. The effect of carbonization via saccharose pyrolysis, which led to a decrease in the impedance and an increase in the diffusion coefficient of lithium to $D = 2.2 \times 10^{-10}$ – 1.7×10^{-9} cm²/s, is studied.

Keywords: lithium-ion batteries, electrochemical impedance spectroscopy, silicon anodes, carbonization, diffusion coefficient of lithium in silicon

DOI: 10.1134/S1063782620030124

1. INTRODUCTION

Silicon is a promising material for the negative electrodes of lithium-ion batteries (LIBs) because it has the highest specific gravimetric capacity (4200 mA h/g), a low incorporation potential of Li (0.2–0.3 V), and it is abundant in Earth's crust. Its disadvantages are a large change in volume upon lithiation, low charge-discharge rate because of the small diffusion coefficient of Li, and instability of the solid-electrolyte interface (SEI) [1]. A method that can slow the degradation rate of silicon electrodes and raise their rate characteristics is the formation of a nanostructured material with submicrometer-element sizes [2], including macroporous silicon constituted by wires or planes retaining the single-crystal structure [3, 4]. It has been shown in intensive studies of new anode materials, carried out around the whole world, that the characteristics of silicon electrodes can be significantly improved via the formation of composites. Of particular interest among these are silicon-carbon composites because they provide a high capacity, high electronic conductivity, and good cycling stability [5, 6].

The method of electrochemical impedance spectroscopy (EIS) is widely used to examine the kinetics of lithium-involving processes [7–10]. In particular, it can be used to find the diffusion coefficient of lithium, which is the most important factor determining the rate capability (charge and discharge time of a battery). The electrochemical lithiation of silicon yields Li_xSi

alloys with a high content of lithium, up to $x = 4.4$. Thus, the diffusion of Li occurs in a variable-composition medium, which affects the mobility of diffusing atoms. The diffusion coefficient measured under these conditions is a concentration-dependent quantity, and it is termed the chemical or effective diffusion coefficient D [11]. Efforts are being made, to correctly find D , to use electrodes made of pure silicon without additional components, most frequently in the form of amorphous Si films [12, 13].

Recently, we have examined the possibility of fabricating macroporous silicon via the cold compression and high-temperature sintering of Si nanopowder in an inert atmosphere [14]. The properties of the material obtained and anodes made of it depend on the structure, which is primarily determined by the temperature and duration of annealing in the course of sintering. Electrodes with the optimal structure had a stable capacity $Q = 1000$ mA h/g (>120 cycles at a charge–discharge rate of C/5), which decreased to 890 mA h/g upon raising the delithiation rate to 1C (C is the unit of battery charge–discharge rate) [15]. Macroporous Si produced by sintering has a crystalline structure and is a convenient object of study by the EIS method. This is so because, in contrast to monolithic materials, it does not disintegrate for a sufficiently long time in the cyclic incorporation and extraction of lithium.

The goal of the present study is to examine by the EIS method the kinetic parameters of sintered Si elec-

Table 1. Parameters of silicon and silicon-carbon electrodes

Parameter	Si	Si/C
L , μm	83	86
m_{Si} , mg	2.72	3.08
ρ_{el} , $\Omega\text{ cm}$	4.1×10^4	45
ρ , g/cm^3	1.34	1.55
p , %	42.5	34
S , mm^2	24.4	23.3

trodes in the lithiated and delithiated state and the influence exerted on these by carbonization.

2. EXPERIMENTAL

Si nanopowder (commercial product from Hongwu Nanometer) constituted by crystalline particles 30–50 nm in diameter served as the initial material. Cold, dry (without a binder) compression was used to form, under a pressure of 180 MPa, pellets with a diameter of 6 mm and $\sim 500\ \mu\text{m}$ thick. Sintering of the pellets was performed at a temperature of $T = 1150^\circ\text{C}$ over 1 h in a flow of argon. This resulted in the coarsening of silicon grains to 150–200 nm and the formation of a connected current-conducting matrix. The gravimetric porosity p of the pellets was determined from the density ρ measured in the study as $p = (1 - \rho/\rho_m) \times 100\%$, where $\rho_m = 2.33\ \text{g/cm}^3$ is the density of monolithic silicon. The electrical resistivity ρ_{el} was measured by the four-probe method. The internal surface area was determined from the nitrogen adsorption isotherm by the BET (Brunauer, Emmett, Teller) method to be $18.6\ \text{m}^2/\text{g}$ [14].

A part of the sintered pellets was saturated with a 45.5% water-ethanol solution of saccharose at a temperature of 70°C for 3 h. Saccharose was pyrolyzed in Ar at $T = 900^\circ\text{C}$ for 1 h. After carbonization, a 20–30- μm -thick layer was removed from both sides of the pellet by grinding. The content of carbon in the Si/C samples was determined by energy-dispersive X-ray microanalysis (EDX) to be 10–15 wt %, with the resistance ρ_{el} decreased by three orders of magnitude.

To form electrodes, copper was electroplated with a thickness of $\sim(20\text{--}30)\ \mu\text{m}$ on one side of the Si or Si/C pellets, and then the thickness of the silicon layer was reduced to $L \approx 85\ \mu\text{m}$. Electrochemical measurements were performed in a laboratory three-electrode cell with a design similar to an HS 3E cell (Honsen), in which the reference and auxiliary electrodes were made of metallic lithium. TC-E918 (Tinci), a 1 M solution of LiPF_6 in a mixture of organic solvents, served as the electrolyte. The galvanostatic charging and discharging of the cell were performed on a CT3008W-5V10mA stand (Neware) at a current density of 0.05 A/g in the first cycle and 0.1 A/g in subsequent cycles. The charging (lithiation) of the elec-

trodes was limited to a capacity of $Q = 1000\ \text{mA h/g}$. Upon the introduction of Li, the voltage applied to the electrode under study relative to the reference electrode was limited to a value of 10 mV, and that upon discharging (extraction of Li), to a voltage of $E = 2\ \text{V}$. The impedance was measured with an AUTOLAB (Metrohm) PGSTAT302N modular potentiostat/galvanostat at frequencies ν in the range from 100 kHz to 0.01 Hz, with the ac voltage amplitude being 5 mV. The impedance spectra were calculated with ZView software (Scribner Associates Inc.). The parameters of the samples for which the impedance measurements were carried out are listed in Table 1, where m_{Si} is the mass of silicon or carbonized silicon, and S is the nominal electrode area.

3. EXPERIMENTAL RESULTS

Figure 1 shows the charge-discharge curves of the samples under study. It is noteworthy that an attempt to introduce lithium at a current of 0.1 A/g failed because the voltage rapidly decreased to 10 mV. The corresponding curves in Figs. 1a and 1b are designated as the zero cycle (0). Therefore, the first lithiation-delithiation cycle was performed at a current of 0.05 A/g. It can be seen that the curve corresponding to the introduction of lithium in the first cycle has a form characteristic of crystalline silicon, with a sharp fall in the voltage and a horizontal plateau [16]. Its shape is determined by the double-phase mechanism of the first embedding of Li, when there is a sharp boundary between the amorphous lithiated $a\text{-Li}_x\text{Si}$ layer and crystalline $c\text{-Si}$ [17]. In this case, the lithiation rate is limited by the reaction at the $a\text{-Li}_x\text{Si}/c\text{-Si}$ interface. After the extraction of lithium, the structure of silicon changes, it becomes amorphous, and subsequent cycles already occur by the single-phase mechanism. This is reflected on the shape of the charging curves, which become more rounded and acquire a nearly linear inclined portion. The irreversible loss of the first cycle, associated with the formation of the SEI, is higher for the Si/C electrode (Coulomb efficiency 75% versus 82% for the Si electrode). This occurs because the surface area becomes larger due to amorphous carbon. In the second and third cycles, the loss decreases in both cases and the Coulomb efficiency increases to 96%.

After each half-cycle of the embedding or extraction of Li, the electrode was disconnected from the stand and relaxed in the open-circuit mode for $\sim(15\text{--}20)\ \text{h}$. After that, the impedance was measured. As a result of relaxation, the voltage on the lithiated electrode increased to a constant value $E_r \approx 0.2\ \text{V}$. The stability of the potential over time after relaxation indicates that a uniform distribution of lithium across the thickness was attained. It can be found from the capacity $Q = 1000\ \text{mA h/g}$ by the formula $Q = 960x$ that the content of lithium in the lithiated sample corresponds to the stoichiometric composition LiSi ($x \approx 1$).

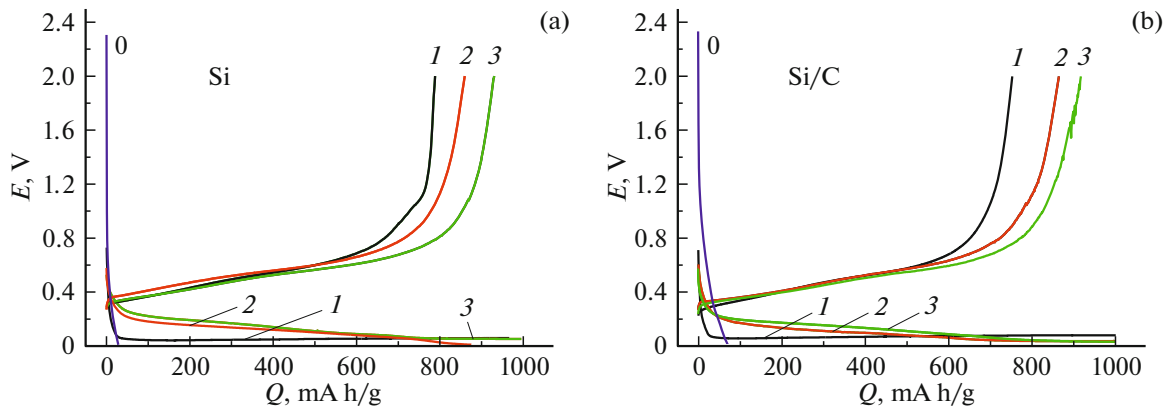


Fig. 1. Charge–discharge curves for (a) Si and (b) Si/C electrodes. The cycle numbers 1, 2, and 3 are indicated.

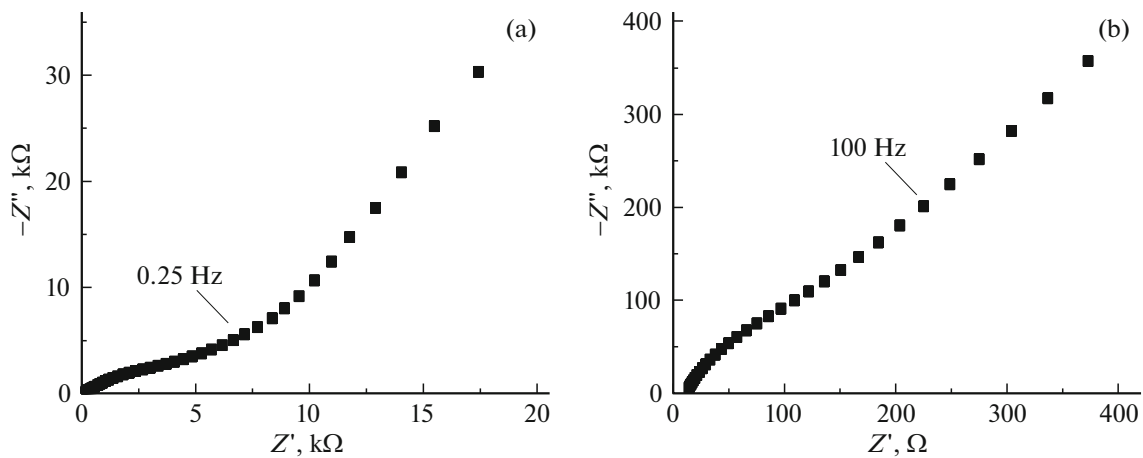


Fig. 2. Impedance spectrum of an un lithiated silicon electrode: (a) general appearance and (b) high-frequency part of the hodograph.

The samples were subjected to a similar procedure after the half-cycle of lithium extraction ($x \approx 0$), complete at $E = 2$ V. In this case, the electrode voltage decreased after relaxation in the open-circuit mode and stabilized at $E_r \approx 0.8$ V.

3.1. Impedance Measurements of Silicon Samples

The measurements began from the impedance spectra $Z' - Z''$ of the initial (un lithiated) electrode. Prior to the measurement, the steady-state potential of the electrode was close to $E = 2$ V. Figure 2 plots the resulting hodograph in Nyquist coordinates. In the absence of embedded lithium, the hodograph has a simple shape, which consists in a half-circle arc that gradually goes to a straight line at low frequencies.

It can be seen in Fig. 3 that the lithiation process leads to a decrease in the impedance and to a change in the shape of the hodograph. Two half-circles are clearly seen in the hodograph in Fig. 3a: a somewhat distorted half-circle with a small diameter at frequen-

cies in the range from 100 kHz to 100 Hz, and a larger diameter half-circle at 100–0.025 Hz. A short linear portion appears at low frequencies. Delithiation leads to an increase in the impedance (Fig. 3b). In this case, the second half-circle clearly observed in the lithiated state, is transformed into a straight line as the frequency decreases. The impedance spectrum for the delithiated state has, on the whole, a shape similar to that observed for the initial electrode. However, a distinct half-circle appears at high frequencies (Fig. 3c). It follows from a comparison of the hodographs in Figs. 3a and 3b that the response of the current to a low-amplitude ac voltage is determined by charge-transfer kinetics in the lithiated state, and by diffusion processes in the delithiated state.

The impedance spectra for subsequent cycles (Fig. 4) do not differ fundamentally from the hodographs for the first cycle and have a similar shape. As the number of cycles increases, the hodographs are shifted to smaller values of the ohmic resistance, which is probably due to loosening of the material.

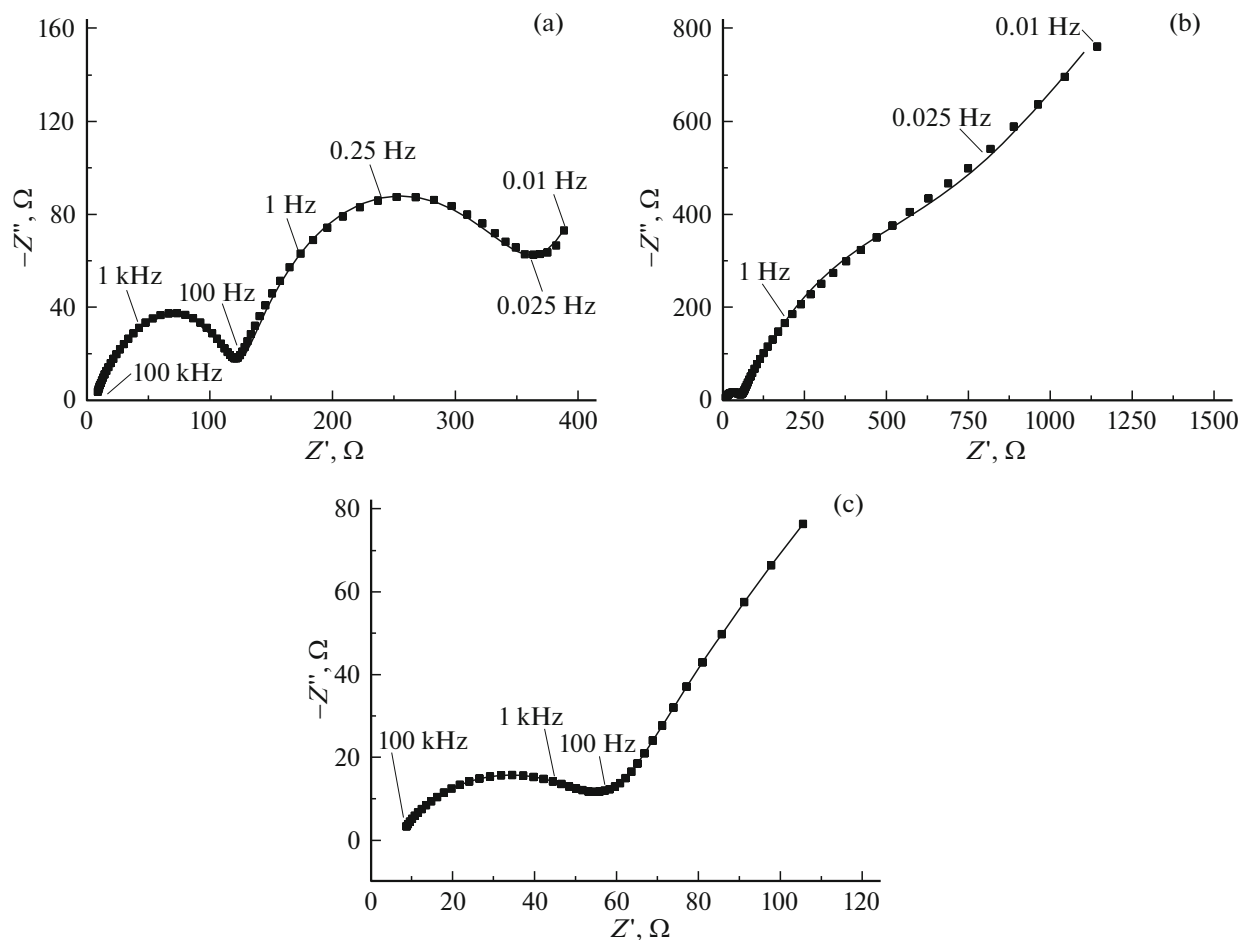


Fig. 3. Impedance hodographs of the Si sample for the first cycle: (a) lithiated state, (b) delithiated state, and (c) high-frequency part of the hodograph for the delithiated state. Points, experimental data; lines, results of calculation for the equivalent circuit. The frequencies ν of the ac voltage are indicated.

The spectra obtained made it possible to suggest the following equivalent electrical circuit shown in Fig. 5.

The circuit has the form of a series-connected resistance R_0 , two parallel combinations of resistance and constant-phase elements ($R_1 \parallel CPE_1$) and ($R_2 \parallel CPE_2$), and the element CPE_3 . The same, or nearly so, equivalent circuits for silicon or composite electrodes were used in [12, 18–20]. The impedance of the constant-phase element was calculated by the formula

$$Z_{CPE} = j/A\omega^n, \quad (1)$$

where j is an imaginary unit $\sqrt{-1}$, $\omega = 2\pi\nu$ is the circular frequency of the measuring signal, and A is a parameter which may correspond, depending on the exponent n , to the resistance ($n = 0$), capacitance ($n = +1$), inductance ($n = -1$) and Warburg impedance coefficient ($n = 0.5$) [21]. The equivalent-circuit parameters at which the best agreement with the EIS

spectra can be obtained for the Si electrode in the first three cycles are listed in Table 2.

The first element of the equivalent circuit is the electrolyte resistance R_0 (or, more precisely, all the ohmic resistances of the system), which is equal to the high-frequency cutoff produced by extrapolation of the hodograph to the real axis. It can be seen in Table 2 that R_0 is nearly independent of the potential and cycle number. The first parallel combination of the resistance R_1 and the constant-phase element CPE_1 simulates the half-circle observed at the highest frequency. The next parallel combination R_2 and CPE_2 belongs to the second clearly distinguishable half-circle in the lithiated state and to the arc of the half-circle (100–0.25 Hz) in the delithiated state (Figs. 3 and 4). Despite the difference of the exponents n_1 and n_2 from unity, both the constant-phase elements CPE_1 and CPE_2 can be interpreted as capacitances, as is done in most studies [12, 20]. The deviation of the exponent from unity is attributed to different factors, e.g., to the

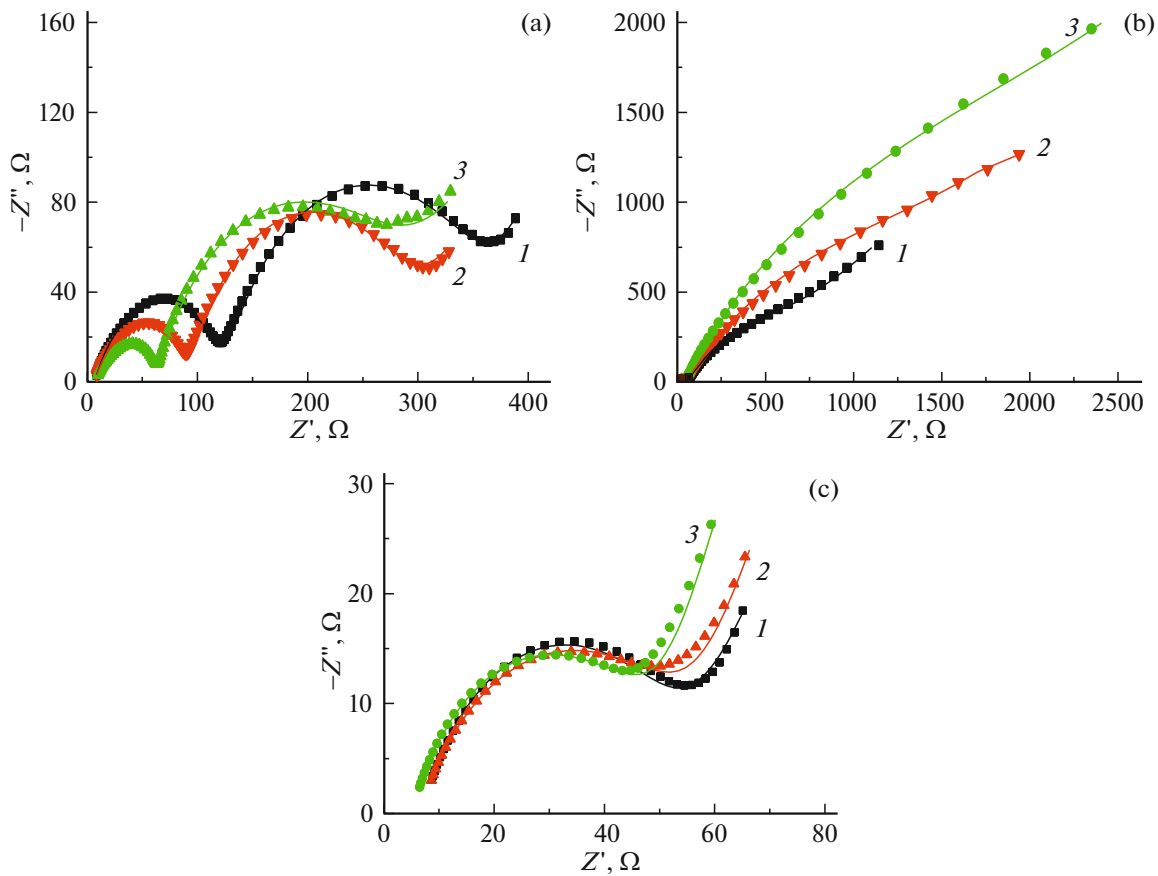


Fig. 4. Changes in the hodographs with increasing cycle number (1, 2, 3): (a) lithiated state, (b) delithiated state, and (c) high-frequency part of the hodograph for the delithiated state. Points, experimental data; lines, results of calculation for the equivalent circuit.

rough surface of the electrode [22] or to the layered structure of the solid-phase SEI film [23–25]. The capacitance A_2 substantially exceeds A_1 , and it can be suggested on this basis that the first parallel combination simulates the SEI, and the second, the electric double layer. Indeed, the capacitance of the electric double layer is, as a rule, one to two orders of magnitude higher than the geometric capacitance of SEI film [26]. The assumption is also confirmed by the comparison of the spectra for the initial electrode and the electrode subjected to the cyclic embedding and extraction of lithium. It can be seen in Figs. 2 and 3 that a half-circle appears at high frequencies only after the first lithiation cycle and is retained in the delithiated state, i.e., this is due to the formation of a SEI. It is noteworthy that the high-frequency half-circle is inherent in many lithium-electrode systems having a passive SEI film [8, 23, 27]. The capacitance of the electric double layer is nearly independent of the potential [23], whereas the charge-transfer resistance sharply grows with increasing potential, as it also does in our case. Thus, it can be supposed that the resistance R_1 characterizes the transport of Li^+ ions across

the SEI, and the parameter A_1 characterizes its geometric capacitance. It is necessary to interpret R_2 as the charge-transfer resistance (rate of the reaction/oxidation of lithium), and A_2 as the capacitance of the electric double layer.

The last element, CPE_3 , simulates the low-frequency linear portion (Warburg impedance), which characterizes the diffusion of lithium ions in the bulk of silicon. It can be seen in Figs. 3 and 4 that the impedance is substantially higher at low frequencies in the delithiated state as compared with the lithiated state, which corresponds to smaller values of parameter A_3 according to formula (1).

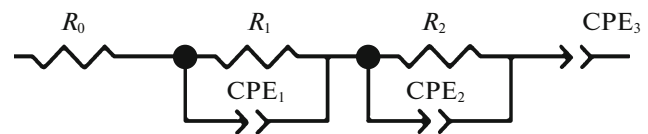


Fig. 5. Equivalent electrical circuit simulating the impedance spectra of Si electrodes.

Table 2. Calculated values of the equivalent-circuit parameters for impedance hodographs in the lithiated and delithiated states of the Si electrode for the first three charge-discharge cycles

State	Lithiated			Delithiated		
	Cycle no.	1	2	3	1	2
R_0, Ω	6.7	6.8	8.5	6.4	6.2	6.1
$A_1, \mu\text{F}$	32.4	44.4	62.4	78.5	50.3	38.8
n_1	0.67	0.64	0.63	0.68	0.64	0.68
R_1, Ω	120	87	53	50	49.6	43.8
$A_2, \mu\text{F}$	2800	2940	3110	2430	2080	1580
n_2	0.77	0.78	0.78	0.69	0.74	0.76
R_2, Ω	230	204	201	617	1110	1800
$A_3, \Omega^{-1} \text{ Hz}^{-n_3}$	0.049	0.070	0.035	0.0061	0.0042	0.0031
n_3	0.61	0.63	0.53	0.6	0.58	0.64

Table 3. Calculated values of the equivalent-circuit parameters for impedance hodographs in the lithiated and delithiated states of the Si/C electrode

State	Lithiated			Delithiated		
	Cycle no.	1	2	3	1	2
R_0, Ω	16.1	17.5	20	24.5	30.2	33.3
$A_1, \mu\text{F}$	52.5	56.8	88	66.6	78	73.4
n_1	0.67	0.61	0.59	0.62	0.65	0.59
R_1, Ω	58.3	54.7	46.7	49.7	25	29.3
$A_2, \mu\text{F}$	2230	2560	2340	3120	3300	3110
n_2	0.83	0.83	0.82	0.7	0.64	0.73
R_2, Ω	148	113	136	226	200	185
$A_3, \Omega^{-1} \text{ Hz}^{-n_3}$	0.081	0.089	0.089	0.0073	0.014	0.0079
n_3	0.55	0.51	0.55	0.6	0.62	0.53

3.2. Impedance Measurements of Carbonized Samples

Figure 6 shows first-cycle impedance hodographs for purely silicon and carbonized electrodes. It can be seen that carbonization leads to a decrease in the impedance. The form of the frequency dependence of the impedance for the composite electrode coincides with that for the silicon electrode, and, therefore, can be simulated with the same equivalent electrical circuit (Fig. 5). The values of the parameters of this circuit for the first three cycles are listed in Table 3.

4. DISCUSSION OF RESULTS

Figure 7 shows how the resistances R_1 and R_2 depend on the cycle number. It can be seen that the

carbonization of a porous Si electrode results in that the resistances R_1 and R_2 decrease in both the lithiated and delithiated states. For both the states, the SEI capacitance A_1 (Tables 2 and 3) increases as a result of carbonization, which is due to an increase in the surface area and agrees with the higher irreversible loss of the capacitance in Si/C in the first cycle. The increase in area is presumably also responsible for the decrease in the resistance R_1 . Irrespective of whether there is or is not a carbon coating, the SEI resistance is, on average, lower in the delithiated state as compared with the lithiated state, which gives reason to believe that the SEI thickness decreases upon the extraction of lithium. This agrees with the effect of a cyclic variation in the SEI thickness, observed in [28, 29]. The decrease in the resistance R_2 , associated with the electrochemical reaction on the surface of silicon grains, i.e., with charge transfer, can be accounted for by an increase in the electronic conductivity as a result of carbonization.

The data furnished by EIS make it possible to determine the effective lithium diffusion coefficient in both the silicon and composite electrodes. The connected structure of the sintered material enables its consideration as a macroscopically homogeneous medium containing defects in the form of pores. Assuming that the embedding and extraction of lithium in Si and Si/C electrodes occurs following the law for semi-infinite diffusion [30], it is possible to find from the linear low-frequency part of the hodograph the slope of the dependence for the imaginary part of the impedance $Z'' = f(\omega^{-0.5})$:

$$-Z'' = \frac{W}{\sqrt{2\pi\nu}}, \quad (2)$$

where W is the Warburg constant.

It can be seen in Fig. 8 that the dependences are well approximated by a straight line. In turn, the Warburg constant is related to the dependence of the equilibrium potential E (V) on the concentration c of diffusing lithium (in mol/cm³) by the expression [30]

$$W = \frac{-dE/dc}{FS\sqrt{2D}}, \quad (3)$$

where D (in cm²/s) is the effective diffusion coefficient of lithium atoms in silicon; F is the Faraday constant (in C/mol); and S is the nominal electrode area (in cm²). dE/dc can be expressed in terms of dE/dQ by using the expression

$$dc = \frac{dQ}{FLS}. \quad (4)$$

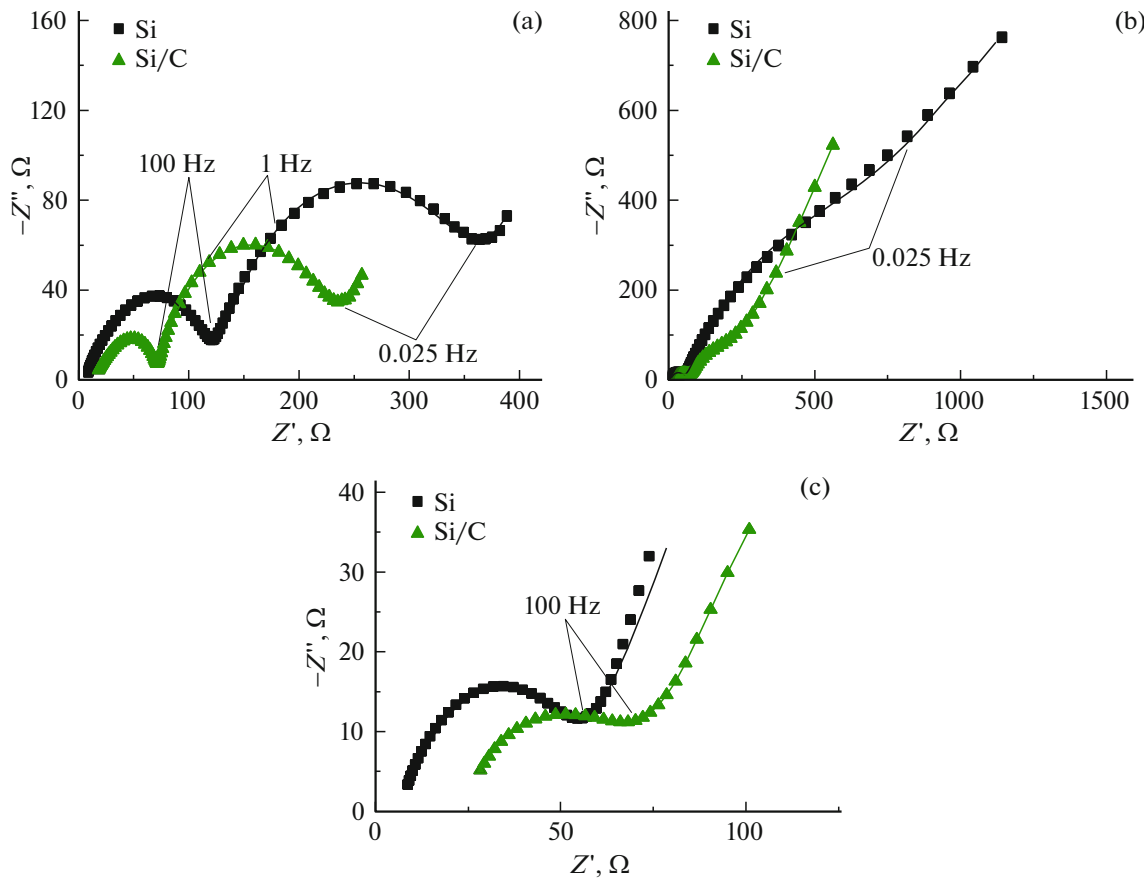


Fig. 6. Impedance hodographs of the Si and Si/C samples for the first cycle: (a) lithiated state, (b) delithiated state, and (c) high-frequency part of the hodograph for the delithiated state.

The combination of equations (3) and (4) gives the following expression for the diffusion coefficient:

$$D = \frac{L^2(dE/dQ)^2}{2W^2}, \quad (5)$$

where L is the electrode thickness in cm.

The value of dE/dQ can be determined from the quasi-equilibrium charge and discharge curves in Fig. 1. The values of dE/dQ , found for the third cycle near $E = 0.2$ and 0.8 V, the Warburg coefficients W , and the lithium diffusion coefficients D , found from these by formula (5), are summarized in Table 4. It is well seen that D is substantially higher in the lithiated

state as compared with the delithiated material. That is, D depends on the content of lithium in the Li_xSi alloy and on the corresponding potential E . A possible reason is an increase in the volume, which occurs when a Li alloy with silicon is formed. The concentration dependence is more strongly pronounced for the purely silicon electrode, compared with that of the composite type. In the latter case, the diffusion coefficient in the delithiated state is substantially (by a factor of ~ 34) larger than that in Si, which can be attributed to the higher mobility of lithium in carbon materials. On the whole, the values we found for D fall within the range 10^{-12} – 10^{-10} cm^2/s , which is in agreement with the published data for silicon [31].

Table 4. Effective lithium diffusion coefficients in silicon and silicon-carbon electrodes, found using EIS

State	Lithiated			Delithiated			
	Parameter	$W, \Omega \text{ s}^{-0.5}$	$dE/dQ, \Omega/\text{s}$	$D, \text{cm}^2/\text{s}$	$W, \Omega \text{ s}^{-0.5}$	$dE/dQ, \Omega/\text{s}$	$D, \text{cm}^2/\text{s}$
Si		9.84	-0.0270	2.6×10^{-10}	479	0.208	6.5×10^{-12}
Si/C		6.11	-0.0414	1.7×10^{-9}	84.2	0.206	2.2×10^{-10}

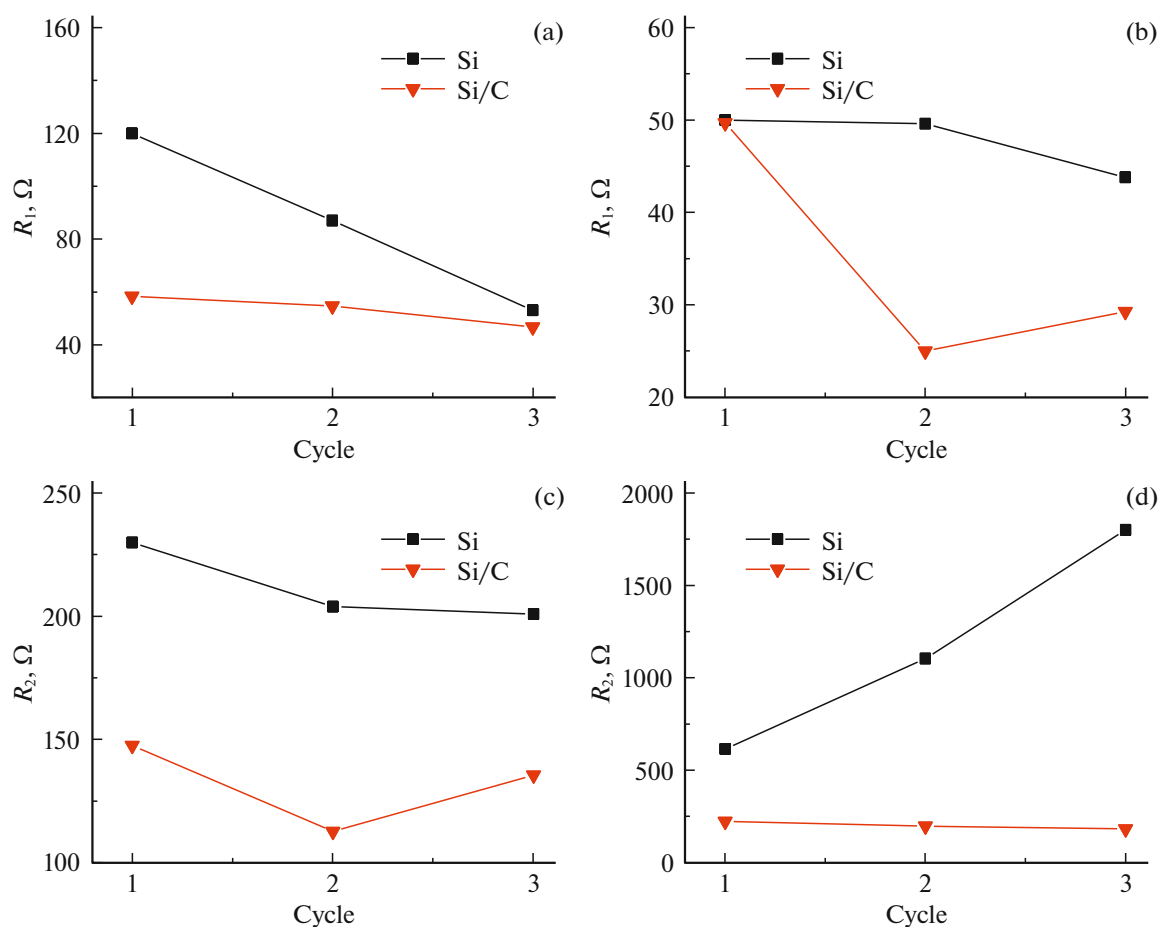


Fig. 7. Effect of carbonization on the resistances (a, b) R_1 and (c, d) R_2 : (a, c) lithiated state and (b, d) delithiated state of the electrode.

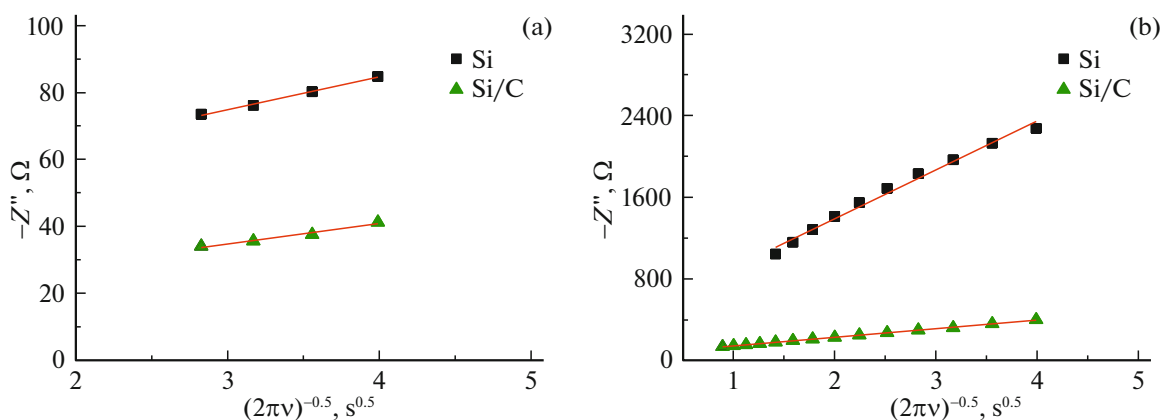


Fig. 8. Dependences of the imaginary part of the impedance on $\sqrt{1/2\pi\nu}$: (a) lithiated state and (b) delithiated state for Si and Si/C electrodes (3rd cycle).

5. CONCLUSIONS

The method of electrochemical impedance spectroscopy was used to find that purely silicon macroporous electrodes produced by the sintering of a nano-

powder and those subjected to additional modification with carbon are characterized by the kinetics of electrochemical processes, typical of other Si and Si/C materials in the form of thin amorphous films of

silicon or composites for the slurry technology. The samples studied exhibit a strong concentration dependence of the effective lithium diffusion coefficient and its significant increase as a result of carbonization. The composite Si/C electrodes possess a lower, compared with Si, charge-transfer resistance and a lower resistance of the SEI film.

CONFLICT OF INTEREST

The authors state that they have no conflict of interest.

REFERENCES

1. J. R. Szczech and Song Jin, *Energ. Environ. Sci.* **4**, 56 (2011).
2. Du Fei-Hu, Wang Kai-Xue, and Chen Jie-Sheng, *J. Mater. Chem. A* **4**, 32 (2016).
3. H. Foll, H. Hartz, E. K. Ossei-Wusu, J. Carstensen, and O. Riemenschneider, *Phys. Status Solidi RRL* **4**, 4 (2010).
4. G. V. Li, E. V. Astrova, A. M. Rumyantsev, V. B. Voronkov, A. V. Parfen'eva, V. A. Tolmachev, T. L. Kulova, and A. M. Skundin, *Russ. J. Electrochem.* **51**, 899 (2015).
5. Liu Xuyan, Zhu Xinjie, and Pan Deng, *R. Soc. Open Sci.* **5** (6), 1 (2018).
6. Dou Fei, Shi Liyi, Chen Guorong, and Zhang Dengsong, *Electrochem. Energy Rev.* **2**, 149 (2019).
7. M. D. Levi and D. Aurbach, *Phys. Chem.* **101**, 4630 (1997).
8. A. V. Churikov, K. I. Pridatko, A. V. Ivanishchev, I. A. Ivanishchev, I. M. Gamayunova, K. V. Zapsis, and V. O. Sycheva, *Russ. J. Electrochem.* **44**, 550 (2008).
9. S. S. Zhang, K. Xu, and T. R. Jow, *Electrochim. Acta* **51**, 1636 (2006).
10. E. Pollak, G. Salitra, V. Baranchugov, and D. Aurbach, *J. Phys. Chem.* **111**, 11437 (2007).
11. W. Weppner and R. A. Huggins, *J. Electrochem. Soc.* **124**, 1569 (1977).
12. T. L. Kulova, Yu. V. Pleskov, A. M. Skundin, E. I. Terukov, and O. I. Kon'kov, *Russ. J. Electrochem.* **42**, 708 (2006).
13. K. Yoshimura, J. Suzuki, K. Sekine, and T. Takamura, *J. Power Sources* **146**, 445 (2005).
14. E. V. Astrova, V. B. Voronkov, A. V. Nashchekin, A. V. Parfent'eva, D. A. Lozhkina, M. V. Tomkovich, and Yu. A. Kukushkina, *Semiconductors* **53**, 530 (2019).
15. E. V. Astrova, V. B. Voronkov, A. M. Rumyantsev, A. V. Nashchekin, A. V. Parfent'eva, and D. A. Lozhkina, *Russ. J. Electrochem.* **55**, 184 (2019).
16. M. N. Obrovac and L. Christensen, *Electrochem. Solid-State Lett.* **7**, 93 (2004).
17. M. Pharr, K. Zhao, X. Wang, Z. Suo, and J. J. Vlassak, *Nano Lett.* **12**, 5039 (2012).
18. R. Ruffo, S. S. Hong, C. K. Chan, R. A. Huggins, and Y. Cui, *J. Phys. Chem.* **113**, 11390 (2009).
19. J. Guo, A. Sun, X. Chen, C. Wang, and A. Manivanan, *Electrochim. Acta* **56**, 3981 (2011).
20. Y. Yamada and Y. Iriyama, *J. Electrochem. Soc.* **157**, 26 (2010).
21. Z. B. Stoinov, B. M. Grafov, B. S. Savova-Stoinova, and V. V. Elkin, *Electrochemical Impedance* (Nauka, Moscow, 1991) [in Russian].
22. *Electroanalytical Methods. Theory and Practice*, Ed. by F. Shol'ts (BINOM, Labor. Znani, Moscow, 2006) [in Russian].
23. M. Umeda, K. Dokko, Y. Fujita, M. Mohamedi, I. Uchida, and J. R. Selman, *Electrochim. Acta* **47**, 885 (2001).
24. D. Aurbach, I. Weissman, A. Schechter, and H. Cohen, *Langmuir* **12**, 3991 (1996).
25. C. Wang, A. J. Appleby, and F. E. Little, *Electrochim. Acta* **46**, 1793 (2001).
26. A. V. Ivanishchev, A. V. Churikov, A. Ivanishcheva, K. V. Zapsis, and I. M. Gamayunova, *Russ. J. Electrochem.* **44**, 510 (2008).
27. D. Aurbach, K. Gamolsky, B. Markovsky, G. Salitra, Y. Gofen, U. Heider, R. Oesten, and M. Schmidt, *J. Electrochem. Soc.* **147**, 1322 (2000).
28. D. Aurbach, B. Markovsky, I. Weissman, E. Levi, and Y. Ein-Ely, *Electrochim. Acta* **45**, 67 (1999).
29. C. K. Chan, R. Ruffo, S. S. Hong, and Y. Cui, *J. Power Sources* **189**, 1132 (2009).
30. C. Ho, I. D. Raistrick, and R. A. Huggins, *J. Electrochem. Soc.* **127**, 343 (1980).
31. F. Ozanam and M. Rosso, *Mater. Sci. Eng.* **213**, 2 (2016).

Translated by M. Tagirdzhanov